Zhujiang Wang
Faculty of Health Sciences,
Ontario Tech University,
Oshawa, ON L1G 0C5, Canada;
Mechanical Engineering and Robotics,
Guangdong Technion-Israel Institute of Technology,
Shantou, Guangdong 515063, China
e-mail: zhujiang.wang@gtiit.edu.cn

Arun Srinivasa
Mechanical Engineering,
Texas A&M University,
College Station, TX 77840
e-mail: arun-r-srinivasa@tamu.edu

J. N. Reddy[1]
Mechanical Engineering,
Texas A&M University,
College Station, TX 77840
e-mail: jnreddy@tamu.edu

Adam Dubrowski
Faculty of Health Sciences,
Ontario Tech University,
Oshawa, ON L1G 0C5, Canada
e-mail: adam.dubrowski@ontariotechu.ca

Topology Optimization of Lightweight Structures With Application to Bone Scaffolds and 3D Printed Shoes for Diabetics

An automatic complex topology lightweight structure generation method (ACTLSGM) is presented to automatically generate 3D models of lightweight truss structures with a boundary surface of any shape. The core idea of the ACTLSGM is to use the PIMesh, a mesh generation algorithm developed by the authors, to generate node distributions inside the object representing the boundary surface of the target complex topology structures; raw lightweight truss structures are then generated based on the node distributions; the resulting lightweight truss structure is then created by adjusting the radius of the raw truss structures using an optimization algorithm based on finite element truss analysis. The finite element analysis-based optimization algorithm can ensure that the resulting structures satisfy the design requirements on stress distributions or stiffness. Three demos, including a lightweight structure for a cantilever beam, a femur bone scaffold, and a 3D shoe sole model with adaptive stiffness, can be used to adjust foot pressure distributions for patients with diabetic foot problems and are generated to demonstrate the performance of the ACTLSGM. The ACTLSGM is not limited to generating 3D models of medical devices, but can be applied in many other fields, including 3D printing infills and other fields where customized lightweight structures are required. [DOI: 10.1115/1.4053396]

Keywords: complex topology structure, truss structure, structure optimization, scaffold, 3D printed shoes, lightweight lattice structures, computational mechanics, stress analysis

1 Introduction

The motivation of this work is to develop an automatic complex topology lightweight structure generation method (ACTLSGM) to generate 3D models of shoe soles for patients with diabetic foot problems. According to the International Diabetes Federation (IDF) statistics, a staggering 537 million people aged 20–79 years are living with diabetes today, and approximately 10% of diabetic patients suffer from diabetic foot and lower limb complications [1]. Patients with diabetes are vulnerable to foot ulcers and long-term severe ulcers can even lead to amputation. A patient's foot pressure distribution is a key factor in preventing and curing diabetes-related ulcers [2]. In the treatment of diabetic foot ulcers (DFUs), offloading is most successful when it mitigates pressure at an area of high vertical or shear stress. Offloading is defined as any measure to eliminate abnormal pressure points to promote healing or prevent recurrence of DFUs [2]. Wearing special shoes and other types of footwear that help distribute a patient's weight is one of the most important ways of offloading to prevent and heal foot wounds. However, such footwear can either be expensive or unesthetic. As the 3D printing and 3D scanning technologies become mature, we propose an alternative solution, 3D printed shoes for diabetics to achieve offloading. To mitigate peak foot pressure, the stiffness shoe soles should be carefully designed. The 3D models of many commercially available 3D printed shoe soles can essentially be considered as complex topology structures, which are adopted widely because such structures can provide precise mechanical properties for personalized shoes due to the ability to grade mechanical properties within a customized volume. Therefore, we focus on developing a method that can automatically create complex topology structures for soles of 3D printed shoes in this work.

Complex topology structures are adopted widely in lightweight infill, porous scaffold, energy absorber, or micro-reactor (energy absorbing, sound attenuating, vibration-isolating, or heat-dissipating) [3,4]. Due to the complex geometry of the structures, designing the 3D models of complex topology structures is challenging. Therefore, researchers and engineers have developed various methods to develop complex topology structure 3D models automatically. The methods can be classified generally into three categories: topology optimization-based method, Boolean operation-based method, and the method that can directly create complex topology structures.

Topology optimization-based complex topology lightweight structure generation method [5] has been used to create lightweight structures with maximum stiffness while reducing material costs. This method has been used in additive manufacturing [6,7], generating aerospace structures [8], and many other fields that require lightweight structures with maximum stiffness regarding prescribed mechanical loads. Zhang et al. [9] presented topology optimization-based lattice structures and obtained a new lattice structure with high load-bearing and energy absorption capacity.

Solid isotropic material with penalization technique and the evolutionary structural optimization (ESO) technique are the most commonly used approaches [10]. The ESO approach [11] is based on gradual material removal from a solid object by repeatedly solving for the stress distribution in the solid using a finite element solver. This is a complicated process requiring heavy computational resources and time.

For the Boolean operation-based complex topology lightweight structure generation methods, a Boolean operation is employed to obtain a target complex topology structure based on a predefined complex topology structure. Cai and Xi [12] proposed Boolean operation-based methods to create porous scaffolds. In this work,

[1]Corresponding author.

Contributed by the Applied Mechanics Division of ASME for publication in the Journal of Applied Mechanics. Manuscript received November 10, 2021; final manuscript received December 22, 2021; published online February 9, 2022. Tech. Editor: Yonggang Huang.

hexahedral mesh and the shape function for finite element methods are employed to control porous geometries. A Boolean operation between solid objects and porous geometries is carried out to generate porous scaffolds. Yoo [13] developed a porous scaffold design method using Boolean operations of the anatomical model and triply periodic minimal surface-based unit cell libraries. Complex pores can be designed with multi-scale complex topology structures.

Additionally, researchers have developed truss structures, Voronoi diagrams, etc. based on methods that can be used to generate complex topology structures directly. For example, in the work by Chen [14], conformal lattice structures with complex topology are generated based on meshes. Nguyen and Vignat [15] developed 3D infills for additive manufacturing, and the infills are generated using meshes used for finite element analysis and unit cell library of lattice structures. Gómez et al. [16] developed bone-like 3D porous scaffolds for tissue engineering using the Voronoi tessellation method. The porosity of the scaffolds can be set to match the main histomorphometric indices of trabecular bone. Wang et al. [17] developed a similar Voronoi tessellation-based porous scaffold generation method and the mechanical properties can be controlled by changing the porosity and irregularity of the nodes distributions for generating Voronoi diagrams. Feng et al. [18] proposed a porous scaffold model generation method using triply periodic minimal surfaces based on T-splines. Yoo [19] developed porous scaffold design through mapping triply periodic minimal surface units from the parametric domain to the space domain. The porosity and internal architecture type are controlled by introducing a hybrid method based on the voxelization algorithm in conjunction with the shape function of the finite element method. Honeycomb-cell structures [20] were another popular complex topology structures that could reduce the material cost and weight of an object while providing a required strength and stiffness. Lu et al. [21] proposed a method that can generate lightweight honeycomb-cell structures as 3D printing infills based on an optimization method using a stress map obtained through finite element analysis. There are many other methods, such as Refs. [22–32], that can directly generate complex topology structures.

Researchers have also developed some hybrid methods. For instance, Wang et al. [33] developed a method to create lightweight truss structures for 3D printing infills. In their work, a raw truss structure is first created and then modified through topology and geometry optimization algorithms.

In this work, we propose an alternative ACTLSGM based on the PIMesh [34,35], which can be used to generate high quality point cloud for meshless methods for an object with any shape.

The core idea of the ACTLSGM is to use a recently developed point cloud generation approach called PIMesh [34] to generate optimally separated node distributions inside the object representing the boundary edge (2D case) or surface (3D case) of the target complex topology structure; raw lightweight truss structures are then generated based on the node distributions; finally, the radius of the raw truss structures is optimized using an optimization algorithm based on finite element analysis.

As the purpose of this work is to develop a method that can be used to generate 3D models of customized shoe soles that can be used as a way of offloading, the stiffness of the shoe soles should be adaptive so as to adjust foot pressure distributions. However, the convectional complex topology lightweight structure generation methods discussed above are aiming at creating overall stiff structures while reducing material cost; therefore, they are not suitable for generating 3D models of customized shoe soles for diabetics. The innovations of this work are

- Compared to conventional complex topology lightweight structure generation methods focusing on generating stiff lightweight structures, the ACTLSGM can generate both stiff lightweight truss structures and structures with adaptive local stiffness.
- As the PIMesh can be used to generate node distributions automatically for an object with any shape, the ACTLSGM can be used to generate a lightweight truss structure with a boundary edge or surface of any shape.
- The finite element truss analysis-based optimization algorithm can adjust the radius of the bars of truss structures according to the stress distributions or the stiffness of the target lightweight structures under predefined mechanical loads at very low computational cost and with very modest computer requirements. This is because of relatively fast computation requiring no remeshing (since the nodes are fixed and simply move based on local conditions and constraints) or other challenges associated with solid-based optimization.

The ACTLSGM is introduced by generating a lightweight truss structure for a cantilever beam at first; a bone scaffold for tissue engineering and a shoe sole model for diabetics are then generated using the ACTLSGM. The details are discussed in the following sections.

Table 1 The overview of the ACTLSGM

1	Prepare the boundary edge (for 2D case) or surface (for 3D case) of the target lightweight truss structure; assign the maximum stress σ_c that is allowed in the truss structure
2	Assign target node distances inside the boundary object
3	Assign nodes inside the object using the PIMesh
4	Generate a raw lightweight truss structure based on the node distributions. Let N be the number of the bars of the truss structure, and $N_{\text{updated}} = N$
5	While $\sigma_{\max} > \sigma_c$ or $N_{\text{updated}} > 0.05N$ (optimize the lightweight truss structure)
5.1	Run finite element analysis to obtain the von Mises stress distributions $\boldsymbol{\sigma}_v$ of the structure, and let $\sigma_{\max} = \max(\boldsymbol{\sigma}_v)$
5.2	Update the diameter of the bars of the truss structure according to the von Mises stress distributions, and N_{updated} is the number of the bars with radius changed
6	Generate the 3D models of the optimized lightweight truss structures

2 Automatic Complex Topology Lightweight Structure Generation Method

The overview of the ACTLSGM is shown in Table 1. To better illustrate the ACTLSGM, a lightweight truss structure is generated for a cantilever beam. As shown in Fig. 1, the solid line segments represent the boundary edges of the cantilever beam, with length $L = 2.0$ m, width $2b = 0.4$ m, and thickness $t = 0.02$ m. The beam is clamped at the left end, and a concentrated force $F = 10$ N is applied at the right end. The goal is to generate a lightweight truss structure composed of steel bars with radius $\boldsymbol{r} = \{1, 2, 3, 4, 5, 6, 7\}$ mm and the maximum von Mises stress of the bars should be smaller than $\sigma_c = 0.5$ MPa.

2.1 Assign Target Node Distances. In the second step of the ACTLSGM, the target distances between nodes that are used for generating a raw lightweight truss structure are assigned for the cantilever beam. To reduce the material usage of a lightweight truss structure, it is expected that the structure is strong where the stress

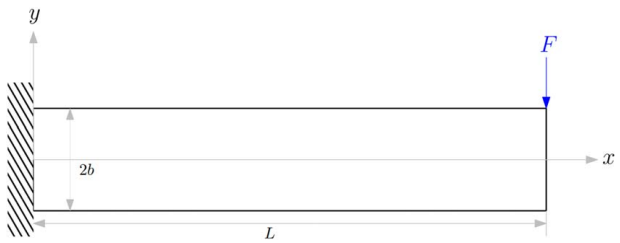

Fig. 1 The plot of the cantilever beam with length $L = 2.0$ m, width $2b = 0.4$ m, and thickness $t = 0.02$ m

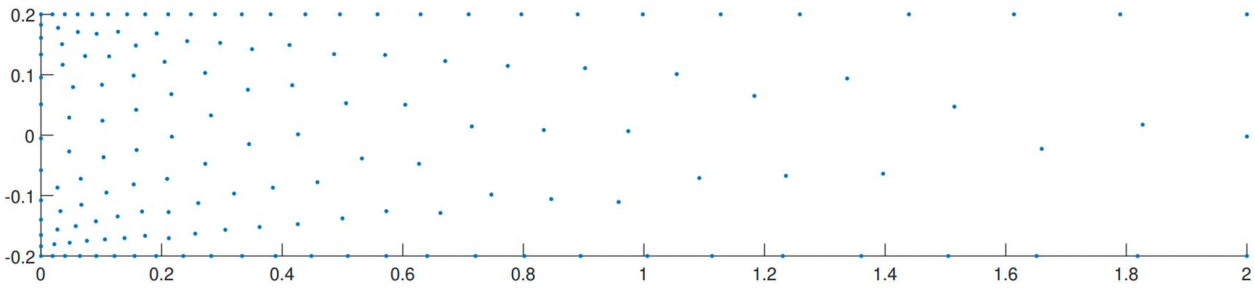

Fig. 2 The node distributions obtained by the PIMesh for the cantilever beam

is large and less strong where the stress is small. Therefore, the von Mises stress of the cantilever beam shown in Fig. 1 and the target node distance should have a negative correlation, because the node distribution is essentially the joints of the lightweight truss structure. As the elastic strain energy caused by bending contributes the majority of the total elastic strain energy of the cantilever beam, the target node distance $h(x, y)$ is set based on the bending stress of the cantilever beam:

$$\begin{aligned} h(x,y) &= h_{\min}(x) + \frac{b-|y|}{b}[h_{\max}(x) - h_{\min}(x)] \\ h_{\min}(x) &= H_{\max} - \frac{\sigma(x)}{\sigma_{\max}}(H_{\max} - H_{\min}) \\ h_{\max}(x) &= \min\{h_{\min}(x) + 0.2b, H_{\max}\} \end{aligned} \tag{1}$$

where $\sigma(x) = M(x)b/I_2$, $M(x) = F(L-x)$, $\sigma_{\max} = M(x)b/I_2$, I_2 the second moments of area of the cantilever beam; $H_{\min} = 0.02$ m is equal to the thickness of the beam, and $H_{\max} = 0.2$ m is equal to half of the width of the cantilever beam.

Table 2 The total number of the bars of the truss structure is $N = 393$, and N_{updated} is the total number of the bars with radius changed

	Round 1	Round 2	Round 3	Round 4
N_{updated}	387	321	73	10

Note: The table shows the N_{updated} at each optimization round.

2.2 Obtaining the Node Distributions Using the PIMesh. Once the target node distances are set, the node distributions are obtained using the PIMesh [34]. The core idea of the PIMesh is that the cantilever beam is considered as an "airtight container" into which nodes are "injected" inside it. The motion of the nodes is controlled by the following formulation:

$$m\ddot{\boldsymbol{x}}_i(t) = \boldsymbol{F}_{fi}(\boldsymbol{x}(t)) + \boldsymbol{F}_{vi}(\dot{\boldsymbol{x}}(t)) \tag{2}$$

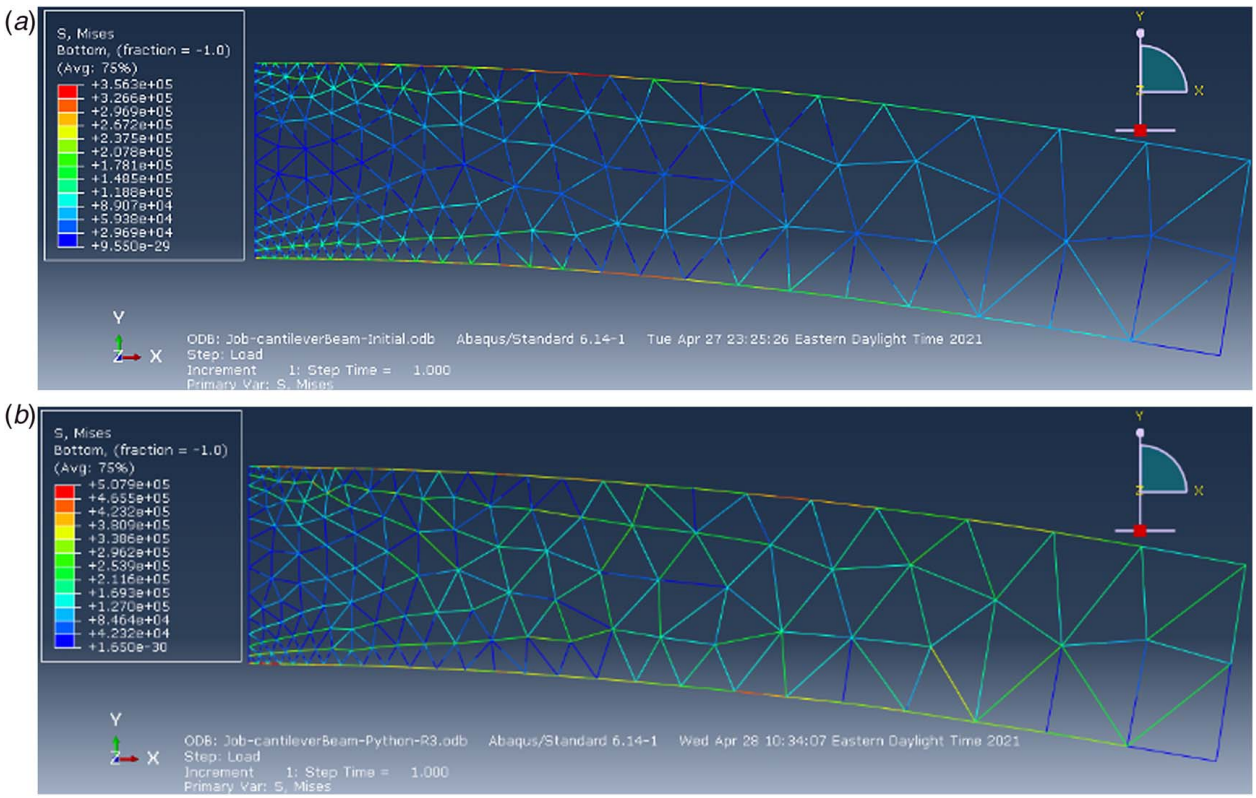

Fig. 3 The von Mises stress distributions over the (*a*) raw and (*b*) optimized lightweight truss structures

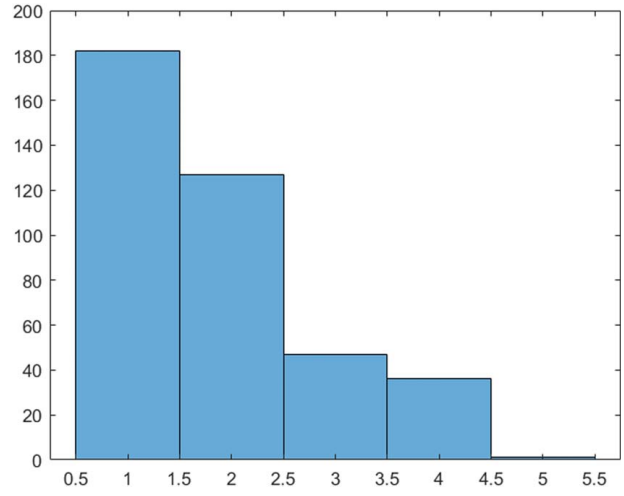

Fig. 4 Histograms of the radius of the optimized lightweight truss structure's bars for the cantilever beam

where the fluid force $\boldsymbol{F}_{fi}$ is

$$\boldsymbol{F}_{fi} = k_s \sum_{j=1}^{N_i} W\left(\frac{\|\boldsymbol{x}_i - \boldsymbol{x}_j\|}{\hat{h}(\boldsymbol{x}_i, \boldsymbol{x}_j)}\right) \frac{\boldsymbol{x}_i - \boldsymbol{x}_j}{\|\boldsymbol{x}_i - \boldsymbol{x}_j\|} \tag{3}$$

where $\boldsymbol{x}_j$ is the positions of the neighbor nodes of the node $\boldsymbol{x}_i$, N_i is the number of the neighbor nodes of $\boldsymbol{x}_i$, $\hat{h}(\boldsymbol{x}_i, \boldsymbol{x}_j)$ is the target distance between node $\boldsymbol{x}_i$ and node $\boldsymbol{x}_j$, $\hat{h}(\boldsymbol{x}_i, \boldsymbol{x}_j) = h(x_i, y_i) + h(x_j, y_j)/2$, $h(x_i, y_i)$ is given in Eq. (1), and $W(q)$ is set as

$$W(q) = \alpha \begin{cases} (2-q)^3 - 4(1-q)^3, & 0 \le q < 1 \\ (2-q)^3, & 1 \le q < 2 \\ 0, & q \ge 2 \end{cases} \tag{4}$$

where $q = \|\boldsymbol{x}_i - \boldsymbol{x}_j\|/\hat{h}(\boldsymbol{x}_i, \boldsymbol{x}_j)$, $\alpha = 1/6$ for 2D case and $\alpha = 1/18$ for 3D case. The viscous force $\boldsymbol{F}_{vi}$ is

$$\boldsymbol{F}_{fi} = -k_v \frac{m\dot{\boldsymbol{x}}}{\Delta t} \tag{5}$$

where Δt is the time-step in the simulation and k_v is a constant ($0 \le k_v < 1$). The viscous force is used to stabilize the fluid nodes motion simulation. When the motion of the nodes is stopped, the positions of the nodes are considered as the node distributions. The node distributions obtained using the PIMesh for the cantilever beam are shown in Fig. 2.

2.3 Generate and Optimize the Truss Structures. After obtaining the node distributions for the cantilever beam, the Delaunay triangulation algorithm is employed to generate a mesh which is used to generate a raw lightweight truss structure for the cantilever beam (each edge of the mesh represents a bar of the truss structure). However, one should note that the raw lightweight truss structure is not limited to Delaunay triangulation-based truss structures. Other structures, such as Voronoi diagram-based lightweight structures and porous lightweight structures, can also be generated based on the node distributions.

The raw lightweight truss structure is shown in Fig. 5(*a*). The radius of the bars of the raw lightweight truss structure is set as $r_{\text{initial}} = 5$ mm. To optimize the raw truss structure, ABAQUS is employed to obtain the von Mises stress distributions of the raw truss structure. In the finite element analysis using ABAQUS, each bar of the truss is assumed to be a beam and the quadratic beam element (ABAQUS element type B22) is employed; as the deformation of the truss structure is assumed to be small, linear simulation is conducted. Once the analysis is completed, the von Mises stresses and the stresses along the bars of the truss structure at the integration points are exported. Because there are two integration points at each bar of the truss structure and at each integration point there are two stresses (one at the top and one at the bottom of a bar's cross section), four von Mises stresses (σ^t_{v1} and σ^b_{v1} at a integration point, σ^t_{v2} and σ^b_{v2} at the other integration point) and four stresses along the bar (σ^t_{x1} and σ^b_{x1} at a integration point, σ^t_{x2} and σ^b_{x2} at the other integration point) are exported for each bar of the truss structure. The truss structure is optimized by adjusting the diameters of the bars of the truss structure according to the following scheme:

- If $\sigma^t_{x1} \cdot \sigma^b_{x1} < 0$ or $\sigma^t_{x2} \cdot \sigma^b_{x2} < 0$ for a bar of the truss structure, the bar is assumed to be under bending load. In this case, the maximum stress is inversely proportional to the second moment of area I_2 (for a bar with a circular cross section, $I_2 = \pi/4\, r^4$), and the radius of the bar of the truss structure is updated as

$$r_{\text{updated}} = \sqrt[4]{\frac{\sigma_{\max}}{\sigma_c}}\, r_{\text{original}}$$

where $\sigma_{\max} = \max\{\sigma^t_{v1}, \sigma^b_{v1}, \sigma^t_{v2}, \sigma^b_{v2}\}$ is the maximum von Mises stress at a bar's integration points.

- If $\sigma^t_{x1} \cdot \sigma^b_{x1} > 0$ or $\sigma^t_{x2} \cdot \sigma^b_{x2} > 0$ for a bar of the truss structure, the bar is assumed to be under either stretching or compressing load. Because the maximum stress is inversely proportional to the area of the cross section of the bar, radius of the bar is updated as

$$r_{\text{updated}} = \sqrt{\frac{\sigma_{\max}}{\sigma_c}}\, r_{\text{original}}$$

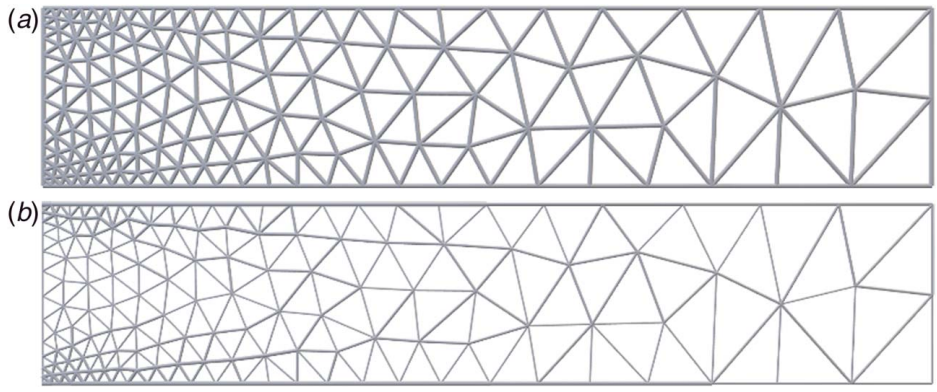

Fig. 5 The (*a*) raw and (*b*) optimized lightweight truss structure for the cantilever beam

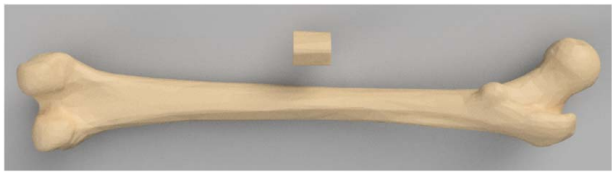

Fig. 6 (Top) The boundary surface of the bone scaffold. (Bottom) A full femur bone.

• (Optional) For the cantilever beam, as the radius of a bar of the truss structure should be among the given set of values $\boldsymbol{r} = \{1, 2, 3, 4, 5, 6, 7\}$ mm, the radius is updated as r_{discrete} (the units of the r_{discrete} is millimeter), where

$$r_{\text{discrete}} = r_{\text{updated}}$$

Note that the maximum $r_{\max} = \max(\boldsymbol{r})$ should be a value ensuring that $\sigma_{\max} < \sigma_c$ for each bar of the truss structure if the radius of the bars of the structure is set as $r_{\max}$.

Once the radius of all the bars of the truss structure is updated, if $\sigma_{\max} \le \sigma_c$ and the total number N_{updated} of the bars with radius changed is smaller than the 5% of the total number of the bars of the truss structure ($N_{\text{updated}} < 0.05$ N), terminate the optimization process; otherwise, repeat steps 5.1 and 5.2 in Table 1.

The cantilever beam truss structure is composed of 393 bars. The optimization took four rounds; at the last round, the radius of 10 bars is updated and the maximum stress in the truss structure is 0.45 MPa which is smaller than $\sigma_c = 0.5$ MPa, and therefore, the optimization procedure is terminated. Table 2 shows the N_{updated} at each optimization round. Figure 3 shows the von Mises stress distributions of the raw and optimized truss structures. Figure 4 shows the histogram of the radius of the bars of the optimized truss structure; compared to the raw lightweight truss structure, the radius of the majority of the bars of the optimized structure is reduced. Figure 5 shows the resulting 3D model of the truss structure for the cantilever beam. The BLENDER 2.8 (open-source software) and PYTHON 3.7 are used to generate 3D models and the details can be found in the work by Wang and Dubrowski [36].

3 Bone Scaffold

In this section, a 3D lightweight truss structure-based bone scaffold for a femur is generated to demonstrate the performance of the ACTLSGM. Scaffolds for tissue engineering have great promise for the future of osseous defects therapies, and porous 3D scaffolds have been utilized to aid and direct bone regeneration. In the past, several works by Feng et al. [18] and Yoo [19] were proposed to create scaffold models. However, verifying the mechanical properties (key factors to guarantee the performance of the scaffolds) of 3D printed scaffolds through experiments is costly. Additionally, it is challenging to design scaffolds with graded mechanical properties [4]. Compared to the traditional work on generating tissue scaffolds, the strength of the resulting scaffolds generated by the ACTLSGM is verified using finite element analysis; furthermore, as the PIMesh can generate nonhomogeneous node distributions, the ACTLSGM can easily generate lightweight structures with graded mechanical properties.

Assume that we need to generate a 3D printed scaffold to replace a piece of a femur bone as shown in Fig. 6, and the scaffold is 3D printed using titanium materials. As the outer compact bone is stronger than the inner spongy bone, the stiffness of an outer layer of the target scaffold is set to be stronger than that of the inner layer of the scaffold to imitate the mechanical properties of a real bone. Therefore, the target node distance for the bone scaffold is set as

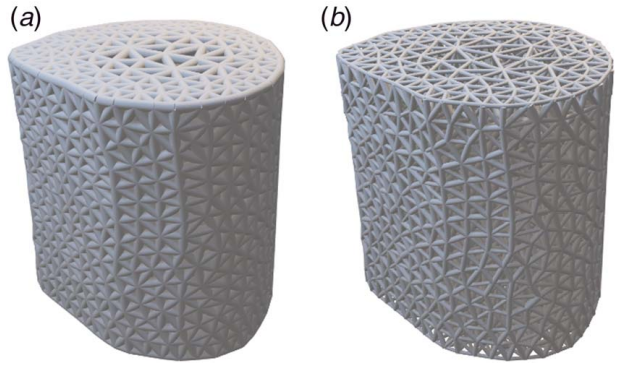

Fig. 7 The (*a*) raw and (*b*) optimized lightweight truss structures for the femur scaffold

$$h(x, y) = \begin{cases} h_{\max} - \dfrac{d}{d_0}(h_{\max} - h_{\min}) & \text{if } d < d_0 \\ h_{\min} & \text{if } d \ge d_0 \end{cases} \tag{6}$$

where $d = \sqrt{x^2 + y^2}$, $d_0 = 10$ mm, $h_{\min} = 2.4$ mm, and $h_{\max} = 8$ mm. With this setting, it is expected that the stiffness of the outer layer is stronger than that of the inner layer of the target structure.

Following the procedure of the ACTLSGM, a raw scaffold model is generated as shown in Fig. 7(*a*), with the radius of the bars of the truss structure set as $r = 0.5$ mm initially. To optimize the structure, in the finite element simulations, Young's modulus of the 3D printed titanium is set as $E = 100$ GPa (note that the material property in this work is an estimation and is only used to demonstrate the performance of the ACTLSGM); a distributed force $N = 1000$ N is applied at one end of the truss structure for the femur bone scaffold and the other end is fixed on a plane; because small deformation is expected, linear analysis in ABAQUS is employed. For the optimization settings, the maximum von Mises stress for each bar of the scaffold is set as $\sigma_c = 50$ MPa, and the radius of each bar of an optimized structure is limited to the given values $\boldsymbol{r} = \{0.1, 0.2, 0.3, 0.4, 0.5, 0.6, 0.7\}$ mm. The optimization is conducted for four rounds. Figure 8 shows the von Mises stress distributions of the initial and optimized structures; Fig. 9 shows the histograms of the radius of the scaffold; Fig. 7(*b*) shows the optimized 3D models of the scaffold. As we can see from Figs. 8 and 9, the maximum von Mises stress is smaller than $\sigma_c = 50$ MPa; the radius of the bars of the optimized structure is much smaller than that of the raw optimized structure; additionally, as the center part of the scaffold is sparser than that of the outer layer, the stiffness of the outer layer of the scaffold should be stronger than that of the inner layer of the scaffold.

4 Shoe Sole Model

The motivation of this work is to generate 3D printable models of shoe soles for diabetics. Patients with diabetic foot problems are very sensitive to foot pressure distribution, which is one of the key factors causing foot ulcers, and adjusting foot pressure distributions for patients is very important in clinical practice. Using a customized 3D printed shoe sole with adaptive stiffness to adjust foot pressure distributions is a promising solution. As 3D printing technologies become mature, one of the key challenges is to generate 3D printable shoe sole models. A complex topology structure is an ideal candidate for the shoe sole model for adjusting foot pressure distributions. However, conventional complex topology lightweight structure generation methods focus on improving the stiffness of lightweight structures while reducing the materials cost and thus are not suitable for generating shoe sole models. In this part, the ACTLGSM is employed to create 3D printable

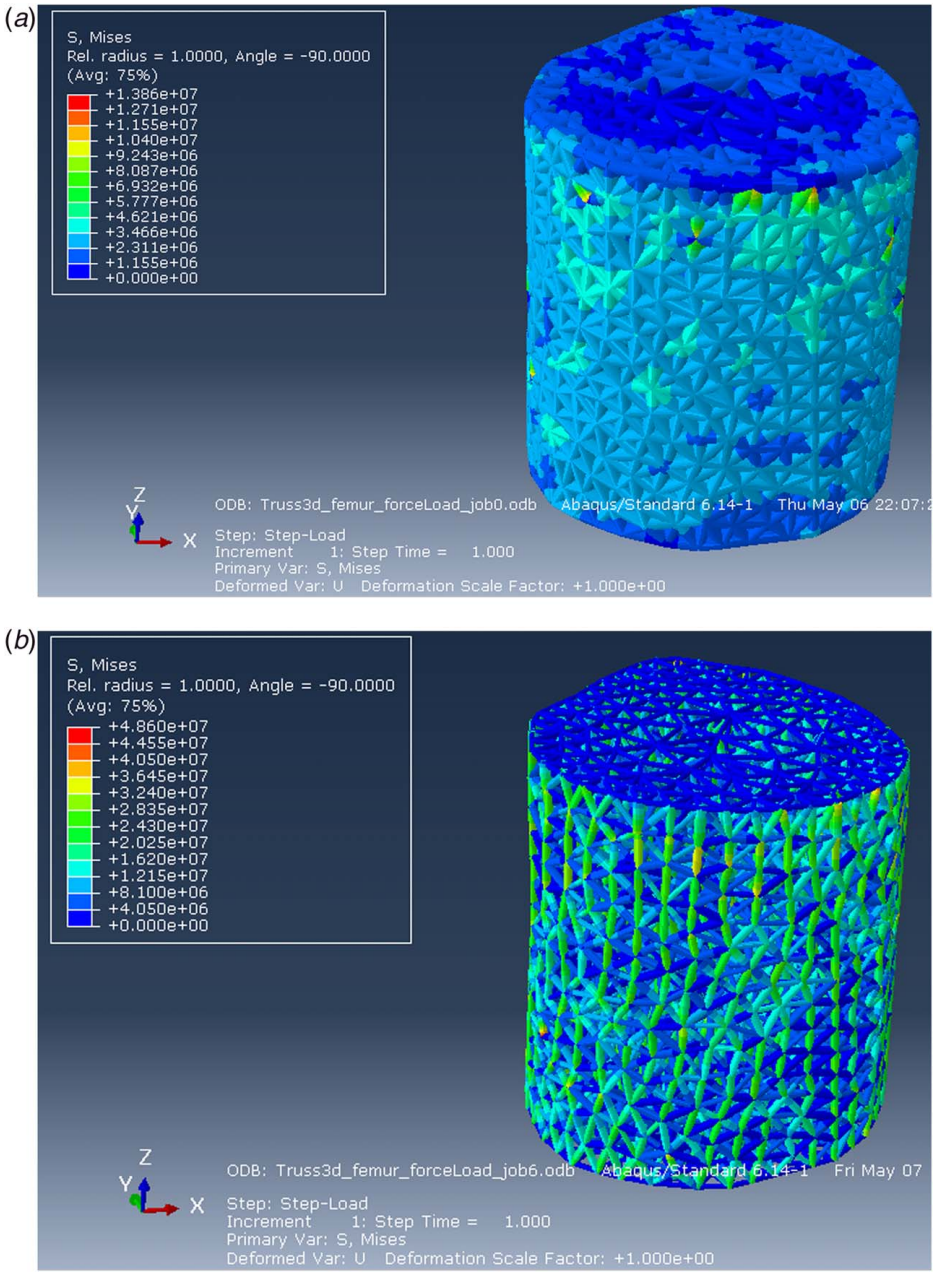

Fig. 8 The von Mises stress distributions over the (*a*) raw and (*b*) optimized bone scaffolds

shoe sole models with adaptive stiffness to reduce peak foot pressure.

Figure 10 shows the bounding surface of the target shoe sole model and Fig. 11 is an assumed foot pressure distribution with peak pressure near forefoot and heel areas. To generate a 3D shoe sole model for relieving the peak foot pressure, the shoe sole should be softer near the forefoot as well as heel areas and stiffer at other areas. Therefore, the node distance should be sparser near the forefoot as well as heal areas and denser at other areas, and the target node distance is set as

$$h(x, y, z) = h_{\min} + \frac{p(x, y) - p_{\min}}{p_{\max} - p_{\min}}(h_{\max} - h_{\min}) \tag{7}$$

where $p(x, y)$ is the assumed pressure distribution shown in Fig. 11; $h_{\max} = 20$ mm; $h_{\min} = 6$ mm; $p_{\max}$ and $p_{\min}$ are the maximum and minimum value of $p(x, y)$, respectively. Following the procedures of the ACTLSGM, a raw shoe sole truss structure composed of bars with a diameter of 1.5 mm is generated. As the goal of this part is to generate a soft shoe sole model with various stiffness while ensuring the shoe sole provides enough support, the von Mises stresses-based optimization method for generating the cantilever beam truss structure and the femur bone scaffold in the previous two sections are not suitable here. The raw shoe sole model is optimized based on the stiffness.

To achieve this goal, in the finite element analysis using ABAQUS, the bottom of the shoe sole model is fixed and a constant force $F = 500$ N is applied on top of the shoe sole model; ABAQUS beam element B32 is employed; the shoe sole is assumed to be printed using TPU95A filaments, and the material is assumed to be elastic with Young's modulus $E = 26$ MPa (note that the material property of the TPU95A in this part is an estimation and is used for demonstrating the performance of the ACTLSGM). After the finite element analysis is completed, instead of exporting von Mises stress, the reaction forces on the top layer of the shoe sole are collected for optimization.

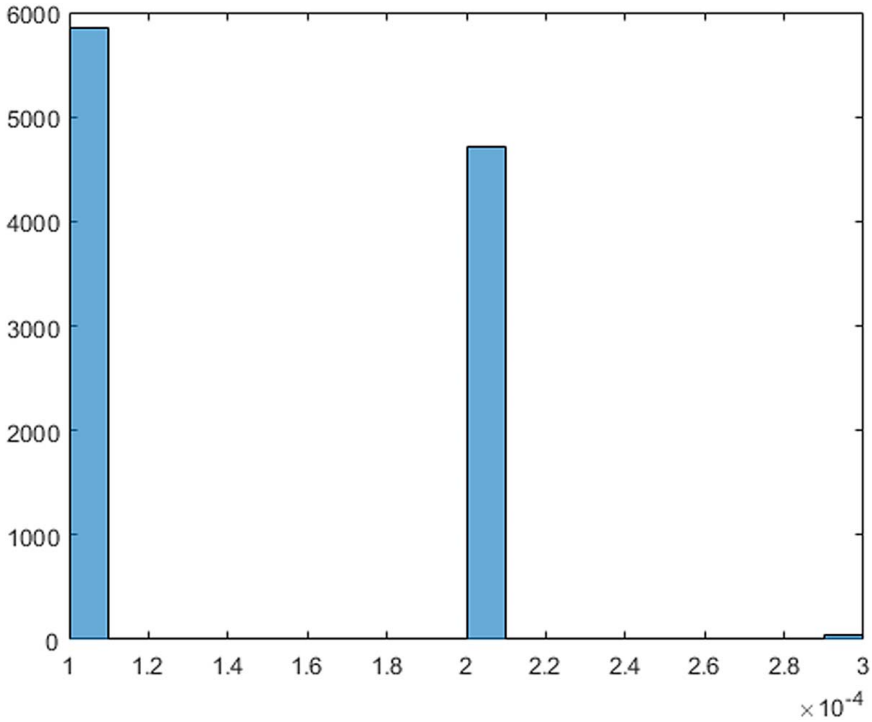

Fig. 9 The histograms of the radius of the bars of the optimized femur scaffold

Fig. 10 The bounding surface of the target shoe sole lightweight structure

Figure 12 shows the reaction forces on the top layer of the raw shoe sole model, and the reaction forces near the forefoot and heel areas are higher than other areas; because our goal is to relieve the peak pressure near the forefoot and heel areas, it is expected that the stiffness of the shoe sole model near these areas is reduced. To reduce the stiffness of the shoe sole model near the forefoot and heel areas, the optimization procedure is modified as

- Obtain the magnitude of the reaction forces F_{ri} at the joints of the top layer of the shoe sole model and calculate the average

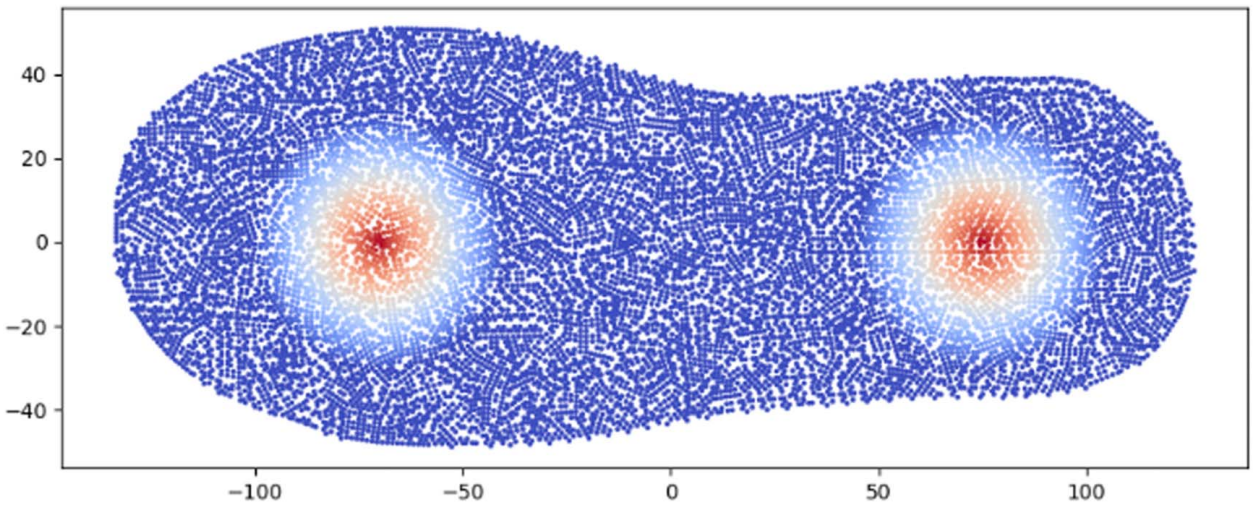

Fig. 11 An assumed foot pressure distribution. Note that the foot pressure distributions may not be realistic, and the purpose to create the pressure distribution is for demoing the performance of the ACTLSGM

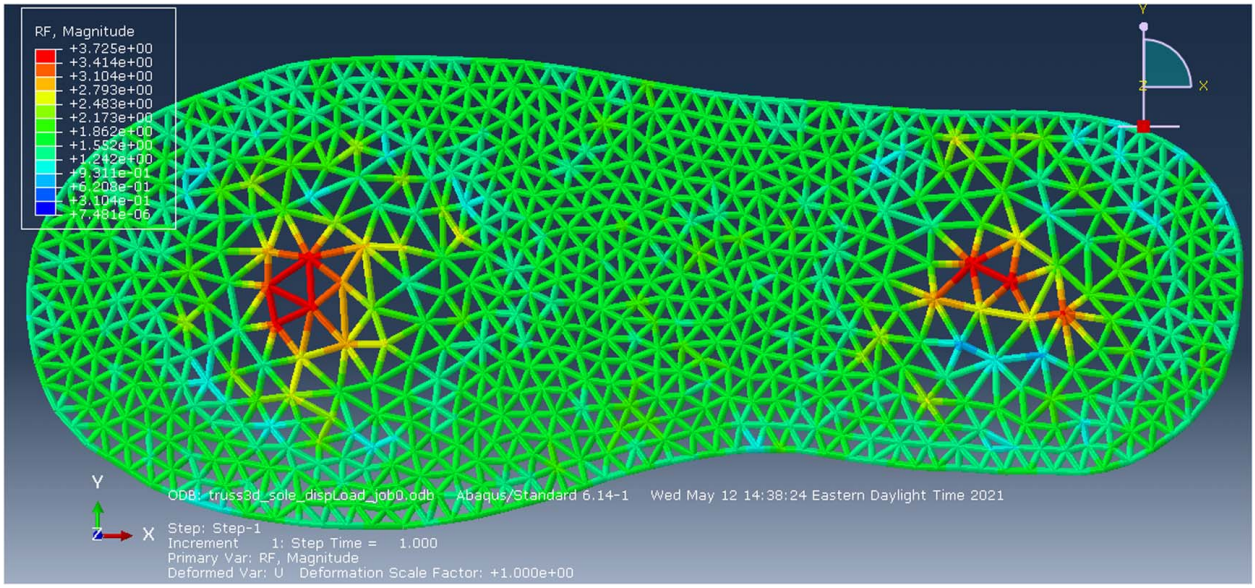

Fig. 12 The reaction forces on the top layer of the raw shoe sole truss structure

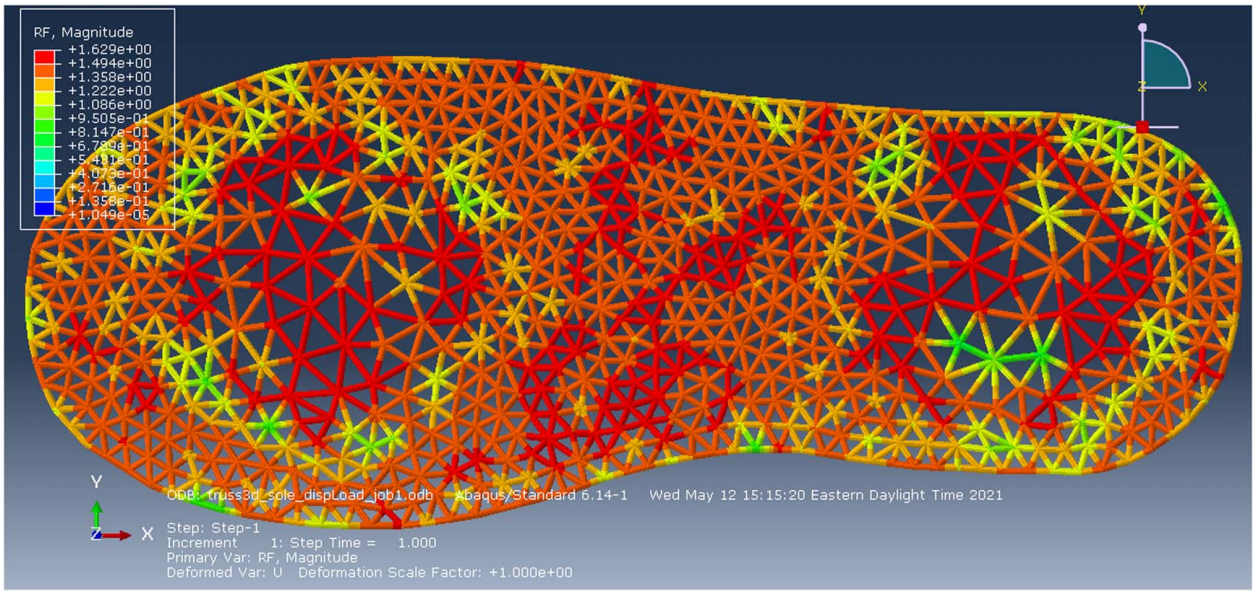

Fig. 13 The reaction forces on the top layer of the optimized shoe sole truss structure

reaction force $F_{\text{avg}} = 1/N \sum_{i=1}^{N} F_{ri}$, where N is the total number of joints at the top layer of the shoe sole model.

- If a reaction force F_{ri} at a joint is greater than the average reaction force F_{avg} ($F_{ri} > F_{\text{avg}}$), find all the bars connected to the joint and update the radius of these bars as

$$r_{\text{updated}} = \sqrt{\frac{F_{\text{avg}}}{F_{ri}}} r_{\text{old}}$$

where r_{old} and r_{updated} are the radius of a bar connecting to the ith joint before and after optimization, respectively.

- Repeat the above procedures until $r_{\max} < r_c$, where $r_{\max} = \max\{\Delta r_1, \Delta r_2, \ldots, \Delta r_N\}$ is the maximum of the radius change of the bars of the truss structure; $\Delta r_i = |r^i_{\text{updated}} - r^i_{\text{old}}|$ is the radius change of the ith bar; $r_c = 0.2$ mm, a typical layer thickness resolution for most commercially available fused deposition modeling 3D printers.

The optimization is conducted for one round (as the maximum of the radius change of the bars of the truss structure is $r_{\max} = 0.18$ mm in the second optimization round, the optimization procedure is terminated). The reaction force on the top layer of the optimized shoe sole structure is shown in Fig. 13, and Fig. 14 shows the histogram of the reaction forces at the joins of the top layer of the raw and optimized shoe sole truss structure. The maximum reaction force is reduced from 1.88 N to 0.94 N after the optimization. The resulting optimized shoe sole lightweight truss structure is shown in Fig. 15.

This project was led by Zhujiang Wang as a part of post-doctoral studies supported by Canada Research Chair in Health Care Simulation awarded to Adam Dubrowski

For a 3D printed shoe, an upper shoe sole is usually covered on top of the shoe sole. To verify the functionality of the shoe sole

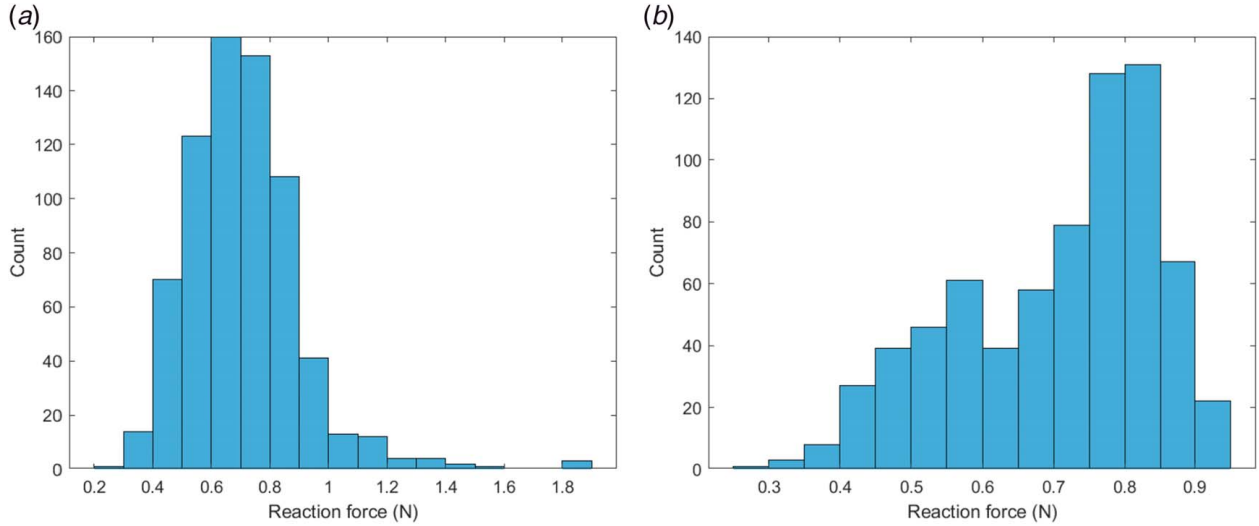

Fig. 14 The histograms of the reaction forces on the layer of the (*a*) raw and (*b*) optimized shoe sole lightweight truss structures

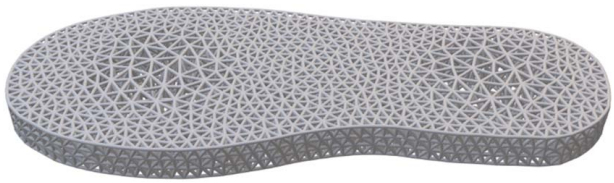

Fig. 15 The optimized shoe sole lightweight truss structure

model, a thin layer TPU95A with a thickness of 1.5 mm is assumed to be attached to the top layer of the shoe sole to smooth foot pressure distribution. Finite element analysis is conducted to analyze the foot pressure distributions using ABAQUS. In the simulation, a uniform displacement load is applied on top of the thin layer material, and the displacement is set as 0.5 mm. Figure 16 shows the reaction force distribution over the top layer material. As we can see from the figure, the reaction forces near the forefoot and heel areas are smaller than other areas, and therefore, the shoe sole is softer near the forefoot and heel areas and stiffer at other areas.

5 Conclusion

In this work, we proposed the ACTLSGM, which can be used to generate stiff lightweight truss structures and lightweight truss structures with adaptive stiffness. The core idea of the ACTLSGM is to use the PIMesh to generate a node distribution and then generate a raw truss structure based on the node distribution; the finite element analysis-based optimization algorithm is then developed to optimize the raw structure by adjusting the radius of each bar of the raw structure according to the requirements in stress distributions or stiffness. Three lightweight truss structures, including the cantilever beam, scaffold, and shoe sole model, are generated to demonstrate the performance of the ACTLSGM. As the PIMesh can generate node distributions for an object with any

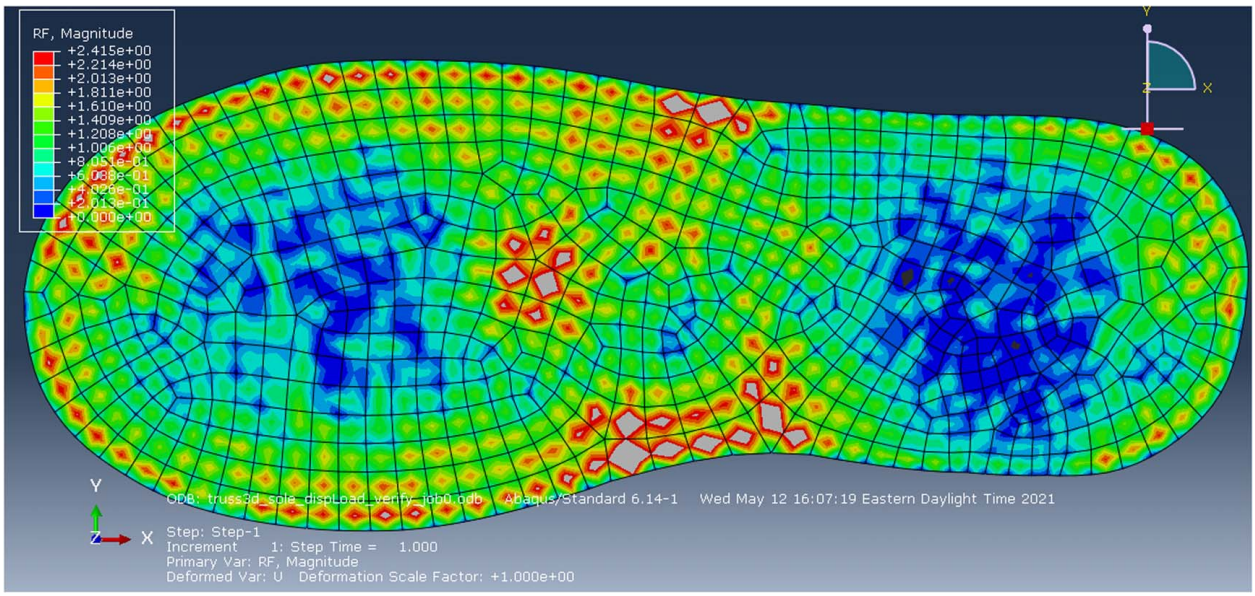

Fig. 16 Reaction force distributions over the TPU95A layer with thickness of 1.5 mm covering the optimized shoe sole truss structure

shape, the ACTLSGM can generate a lightweight truss structure with any boundary shape. The finite element analysis-based optimization method ensures that the lightweight truss structure satisfies the desired design requirements. However, the ACTLSGM is not limited to generate truss structures. Once obtained, the node distributions, porous structure, and Voronoi diagram-based truss structures could also be generated.

In the future, we will develop customized 3D printed shoes for patients with diabetes to prevent and cure diabetic foot problems and explore the generation of porous structures and Voronoi diagram-based truss structures using the ACTLSGM. Because the applications of the ACTLSGM are not limited to 3D printed scaffolds and shoe soles, we will explore other potential applications of the ACTLSGM in customized medical devices, civilian engineering, 3D printing infills, aerospace engineering, etc., where customized lightweight structures are required.

Acknowledgment

The first and last authors gratefully acknowledge the support of the program of Canada Research Chair in Health Care Simulation. This project was led by Zhujiang Wang as a part of post-doctoral studies supported by Canada Research Chair in Health Care Simulation awarded to Adam Dubrowski. The second and third authors acknowledge the support of the [redacted] in the performance of this work.

Conflict of Interest

There are no conflicts of interest.

Data Availability Statement

The datasets generated and supporting the findings of this article are obtainable from the corresponding author upon reasonable request. The authors attest that all data for this study are included in the paper.

References

[1] International Diabetes Federation, 2021, *IDF Diabetes Atlas*, 10th edn. Brussels, Belgium. [Internet]. [cited 2021 Dec 16]. https://www.diabetesatlas.org
[2] Bus, S. A., van Deursen, R. W., Armstrong, D. G., Lewis, J. E. A., Caravaggi, C. F., and Cavanagh, P. R., 2016, "Footwear and Offloading Interventions to Prevent and Heal Foot Ulcers and Reduce Plantar Pressure in Patients With Diabetes: A Systematic Review," Diabetes/Metab. Res. Rev., **32**(S1), pp. 99–118.
[3] Pan, C., Han, Y., and Lu, J., 2020, "Design and Optimization of Lattice Structures: A Review," Appl. Sci., **10**(18), p. 6374.
[4] Lv, Y., Wang, B., Liu, G., Tang, Y., Lu, E., Xie, K., Lan, C., Liu, J., Qin, Z., and Wang, L., 2021, "Metal Material, Properties and Design Methods of Porous Biomedical Scaffolds for Additive Manufacturing: A Review," Front. Bioeng. Biotechnol., **9**, p. 194.
[5] Sigmund, O., and Maute, K., 2013, "Topology Optimization Approaches," Struct. Multidiscipl. Optim., **48**(6), pp. 1031–1055.
[6] Wu, J., Clausen, A., and Sigmund, O., 2017, "Minimum Compliance Topology Optimization of Shell–Infill Composites for Additive Manufacturing," Comput. Methods Appl. Mech. Eng., **326**, pp. 358–375.
[7] Wu, J., 2018, "Continuous Optimization of Adaptive Quadtree Structures," Comput. Aided Des., **102**, pp. 72–82.
[8] Zhu, J.-H., Zhang, W.-H., and Xia, L., 2016, "Topology Optimization in Aircraft and Aerospace Structures Design," Arch. Comput. Methods Eng., **23**(4), pp. 595–622.
[9] Zhang, L., Song, B., Fu, J. J., Wei, S. S., Yang, L., Yan, C. Z., Li, H., Gao, L., and Shi, Y. S., 2020, "Topology-Optimized Lattice Structures With Simultaneously High Stiffness and Light Weight Fabricated by Selective Laser Melting: Design, Manufacturing and Characterization," J. Manuf. Process., **56**, pp. 1166–1177.
[10] Bendsoe, M. P., and Sigmund, O., 2003, *Topology Optimization: Theory, Methods, and Applications*, Springer Science & Business Media, Berlin/Heidelberg, p. 392.
[11] Xie, Y. M., and Steven, G. P., 1993, "A Simple Evolutionary Procedure for Structural Optimization," Comput. Struct., **49**(5), pp. 885–896.
[12] Cai, S., and Xi, J., 2008, "A Control Approach for Pore Size Distribution in the Bone Scaffold Based on the Hexahedral Mesh Refinement," Comput. Aided Des., **40**(10), pp. 1040–1050.
[13] Yoo, D. J., 2011, "Porous Scaffold Design Using the Distance Field and Triply Periodic Minimal Surface Models," Biomaterials, **32**(31), pp. 7741–7754.
[14] Chen, Y., 2006, "A Mesh-Based Geometric Modeling Method for General Structures," Proceedings of the ASME 2006 International Design Engineering Technical Conferences and Computers and Information in Engineering Conference, 26th Computers and Information in Engineering Conference, Vol. 3, ASME, Philadelphia, PA, Sept. 10–13, pp. 269–281.
[15] Nguyen, D. S., and Vignat, F., 2016, "A Method to Generate Lattice Structure for Additive Manufacturing," IEEE International Conference on Industrial Engineering and Engineering Management (IEEM), Bali, Indonesia, pp. 966–970.
[16] Gómez, S., Vlad, M. D., López, J., and Fernández, E., 2016, "Design and Properties of 3D Scaffolds for Bone Tissue Engineering," Acta Biomater., **42**, pp. 341–350.
[17] Wang, G., Shen, L., Zhao, J., Liang, H., Xie, D., Tian, Z., and Wang, C., 2018, "Design and Compressive Behavior of Controllable Irregular Porous Scaffolds: Based on Voronoi-Tessellation and for Additive Manufacturing," ACS Biomater. Sci. Eng., **4**(2), pp. 719–727.
[18] Feng, J., Fu, J., Shang, C., Lin, Z., and Li, B., 2018, "Porous Scaffold Design by Solid T-Splines and Triply Periodic Minimal Surfaces," Comput. Methods Appl. Mech. Eng., **336**, pp. 333–352.
[19] Yoo, D.-J., 2012, "Heterogeneous Porous Scaffold Design for Tissue Engineering Using Triply Periodic Minimal Surfaces," Int. J. Precis. Eng. Manuf., **13**(4), pp. 527–537.
[20] Feng, J., Fu, J., Lin, Z., Shang, C., and Li, B., 2018, "A Review of the Design Methods of Complex Topology Structures for 3D Printing," Vis. Comput. Ind. Biomed. Art., **1**(1), p. 5.
[21] Lu, L., Sharf, A., Zhao, H., Wei, Y., Fan, Q., Chen, X., Savoye, Y., Tu, C., Cohen-Or, D., and Chen, B., 2014, "Build-to-Last: Strength to Weight 3D Printed Objects," ACM Trans. Graph., **33**(4), pp. 1–10.
[22] Martínez, J., Song, H., Dumas, J., and Lefebvre, S., 2017, "Orthotropic k-Nearest Foams for Additive Manufacturing," ACM Trans. Graph., **36**(4), pp. 1–12.
[23] Zhang, X., Xia, Y., Wang, J., Yang, Z., Tu, C., and Wang, W., 2015, "Medial Axis Tree—An Internal Supporting Structure for 3D Printing," Comput. Aided Geom. Des., **35**, pp. 149–162.
[24] Medeirose Sá, A., Mello, V. M., Rodriguez Echavarria, K., and Covill, D., 2015, "Adaptive Voids," Vis. Comput., **31**(6), pp. 799–808.
[25] Tang, Y., Kurtz, A., and Zhao, Y. F., 2015, "Bidirectional Evolutionary Structural Optimization (BESO) Based Design Method for Lattice Structure to be Fabricated by Additive Manufacturing," Comput. Aided Des., **69**, pp. 91–101.
[26] Aremu, A. O., Brennan-Craddock, J. P. J., Panesar, A., Ashcroft, I. A., Hague, R. J., Wildman, R. D., and Tuck, C., 2017, "A Voxel-Based Method of Constructing and Skinning Conformal and Functionally Graded Lattice Structures Suitable for Additive Manufacturing," Addit. Manuf., **13**, pp. 1–13.
[27] Li, D., Dai, N., Jiang, X., and Chen, X., 2016, "Interior Structural Optimization Based on the Density-Variable Shape Modeling of 3D Printed Objects," Int. J. Adv. Manuf. Technol., **83**(9), pp. 1627–1635.
[28] Gorguluarslan, R. M., Gandhi, U. N., Song, Y., and Choi, S.-K., 2017, "An Improved Lattice Structure Design Optimization Framework Considering Additive Manufacturing Constraints," Rapid Prototyp. J., **23**(2), pp. 305–319.
[29] Martínez, J., Hornus, S., Song, H., and Lefebvre, S., 2018, "Polyhedral Voronoi Diagrams for Additive Manufacturing," ACM Trans. Graph., **37**(4), pp. 1–15.
[30] Ion, A., Kovacs, R., Schneider, O. S., Lopes, P., and Baudisch, P., 2018, "Metamaterial Textures," Proceedings of the 2018 CHI Conference on Human Factors in Computing Systems, Association for Computing Machinery, New York, Apr. 1–12, pp. 1–12.
[31] Zhang, X.-Y., Yan, X.-C., Fang, G., and Liu, M., 2020, "Biomechanical Influence of Structural Variation Strategies on Functionally Graded Scaffolds Constructed With Triply Periodic Minimal Surface," Addit. Manuf., **32**, p. 101015.
[32] Ma, S., Song, K., Lan, J., and Ma, L., 2020, "Biological and Mechanical Property Analysis for Designed Heterogeneous Porous Scaffolds Based on the Refined TPMS," J. Mech. Behav. Biomed. Mater., **107**, p. 103727.
[33] Wang, W., Wang, T. Y., Yang, Z., Liu, L., Tong, X., Tong, W., Deng, J., Chen, F., and Liu, X., 2013, "Cost-Effective Printing of 3D Objects With Skin-Frame Structures," ACM Trans. Graph., **32**(6), pp. 1–10.
[34] Wang, Z., Srinivasa, A., Reddy, J. N., and Dubrowski, A., 2021, "PIMesh: An Automatic Point Cloud and Unstructured Mesh Generation Algorithm for Meshless Methods and Finite Element Analysis," Int. J. Numer. Methods Biomed. Eng.
[35] Wang, Z., Srinivasa, A. R., Reddy, J. N., and Dubrowski, A., 2021, "FlowMesher: An Automatic Unstructured Mesh Generation Algorithm With Applications from Finite Element Analysis to Medical Simulations," ArXiv210305640.
[36] Wang, Z., and Dubrowski, A., 2021, "A Semi-Automatic Method to Create an Affordable Three-Dimensional Printed Splint Using Open-Source and Free Software," Cureus, **13**(3), pp. 1–11.